Journal of King Saud University – Computer and Information Sciences 35 (2023) 101648

HOSTED BY

Contents lists available at ScienceDirect

Journal of King Saud University – Computer and Information Sciences

journal homepage: www.sciencedirect.com

Graph adaptive semi-supervised discriminative subspace learning for EEG emotion recognition

Fengzhe Jin [a], Yong Peng [a,b,*], Feiwei Qin [a], Junhua Li [c], Wanzeng Kong [a,b]

[a] School of Computer Science and Technology, Hangzhou Dianzi University, Hangzhou 310018, China
[b] Zhejiang Key Laboratory of Brain-Machine Collaborative Intelligence, Hangzhou 310018, China
[c] School of Computer Science and Electronic Engineering, University of Essex, Colchester CO4 3SQ, UK

ARTICLE INFO

Article history:
Received 25 April 2023
Revised 2 July 2023
Accepted 5 July 2023
Available online 10 July 2023

Keywords:
Discriminative subspace learning
Electroencephalogram (EEG)
Emotion recognition
Maximum entropy graph
Semi-supervised learning

ABSTRACT

Since Electroencephalogram (EEG) is resistant to camouflage and contains abundant neurophysiological information, it shows significant superiorities in objective emotion recognition, making EEG-based emotion recognition become a hot research field in brain-computer interface research. However, EEG is generally non-stationary and has a low signal-to-noise ratio, which is difficult to analyze. Inspired by the consensus that exploring a discriminative subspace representation usually helps to capture the semantic information of EEG data, in this paper we propose a Graph Adaptive Semi-supervised Discriminative Subspace Learning (GASDSL) model for EEG-based emotion recognition. GASDSL aims to explore a discriminative subspace in which the intra-class scatter decreases while the inter-class separability increases. The adaptive maximum entropy graph construction and semi-supervised subspace emotional state prediction are adopted to mediate the discriminative subspace learning. Extensive comparative studies on the SEED-IV and SEED-V datasets depict that 1) GASDSL achieved satisfactory emotion recognition accuracy compared with other semi-supervised learning models, 2) the discriminative abilities of both the learned maximum entropy graph and subspace are improved as the model iterates, and 3) the features extracted from the *Gamma* band, the left/right temporal, prefrontal, and (central) parietal lobes contributed more to emotion recognition based on the spatial-frequency pattern analysis results.

1. Introduction

Emotion plays an important role in interpersonal communication and people make behavioral decisions through emotional interaction. Emotion recognition has become the research hotspot in many fields such as the cognitive science and neural engineering (Li et al., 2022e). In the field of artificial intelligence, endowing machine the ability of understanding human emotional states is of great significance to achieve affective brain-computer interfaces. Current research on emotion recognition is primarily based on non-physiological signals such as facial expressions, speech, and text (Tang et al., 2023). However, emotions might be not externalized in faces or speech and research have shown that it is inaccurate to judge emotional states from non-physiological signals (Wu et al., 2023). On one hand, the way people expresses their emotions changes with different cultures and experiences. On the other hand, people can hide their true emotional state by deliberately disguising their facial expressions or changing the tone of their voices. EEG data is the scalp reflection of central neural activities and occurs spontaneously with emotions, which has been a reliable data source for emotion recognition. With the rapid development of weak signal acquisition equipment and analysis technology, EEG data has been involved in multiple studies and applications such as fatigue detection (Wang et al., 2020), instrument control (Li et al., 2020), emotion recognition (Li et al., 2022f, and mental workload assessment (Kakkos et al., 2021). In this work, our focus is the EEG-based emotion recognition.

As shown in Fig. 1, EEG-based emotion recognition system is generally composed of four parts, *i.e.*, signal acquisition, signal processing, feature extraction, and emotion recognition, among which the latter two stages are the current research hotpsots. Recently, diverse methods were proposed for improving the performance

* Corresponding author at: School of Computer Science and Technology, Hangzhou Dianzi University, Hangzhou 310018, China.
E-mail address: yongpeng@hdu.edu.cn (Y. Peng).
Peer review under responsibility of King Saud University.

Production and hosting by Elsevier

https://doi.org/10.1016/j.jksuci.2023.101648
1319-1578/

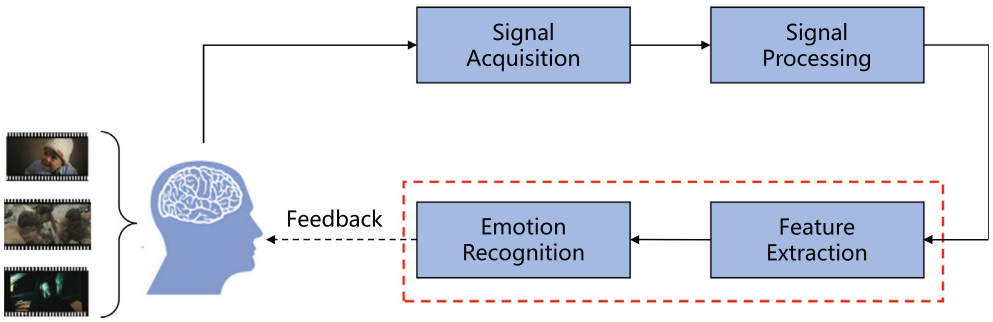

Fig. 1. Flowchart of the EEG-based closed-loop emotion recognition system.

of EEG-based emotion recognition from two aspects, *i.e.*, feature extraction (Zhang et al., 2019), machine learning-based feature learning and recognition (Gu et al., 2021). Generally, feature extraction methods aim to extract powerful features to capture the spatial-frequency-temporal information of EEG data as much as possible. In Gao et al. (2022), a supervised dimensionality reduction method was designed on the Riemannian manifold to reduce the high dimensionality of the symmetric positive definite (SPD) metrices, which were constructed by the time–frequency features of the EEG signals. Similarly, the wavelet analysis is used for EEG-based emotion recognition by sufficiently exploring the time–frequency information from EEG data (Islam and Ahmad, 2019). To simultaneously make use of the complementary information provided by multi-modal data, a multi-modal emotion database (MED4) was collected for EEG emotion recognition, which consists of synchronously recorded EEG signals, photoplethysmography, speech and facial images (Wang et al., 2022c).

For machine learning models, they usually perform linear or nonlinear feature transformation to enhance their discriminative ability for subsequent classification. In Li et al. (2022d), an ensemble learning method based on multiple objective particle swarm optimization was proposed for subject-independent EEG-based emotion recognition. Some deep neural networks completes feature learning and recognition in an end-to-end manner by taking raw EEG data as input and directly outputting the emotion recognition results (Gong et al., 2022). Based on the capsule network and the attension mechanism, a multi-task learning framework was proposed to improve the model generalization and robustness in EEG-based emotion recognition (Li et al., 2022a). In Wei et al. (2023), a Transformer Capsule Network (TC-Net) was proposed for emotion recognition, which contains an EEG Transformer module to extract EEG features and an Emotion Capsule module to refine features and classify the emotional states. By combining a multi-scale residual network with a meta-transfer learning strategy, it shows that not only the relationship between connectivity features and emotional states were explored but also the problem of inter-subject differences was alleviated (Li et al., 2022c). In Wu et al. (2022), the multi-scale bi-hemispheric asymmetric model based on convolutional neural network structure was proposed, which is inspired by the multi-scale characteristics of the EEG data and the neural mechanisms of the emotion cognition.

Though rapid progresses were made within the field of EEG-based emotion recognition, there still have some shortcomings that need to be further improved, two among which are investigated mainly in this paper. One is that EEG data in high-dimensional representation often consists of both redundant and noisy features. An intuitive and effective way is projecting EEG data into a low-dimensional subspace for reducing the dimensionality and simultaneously enhancing the discriminative ability. Adaptive selection of features is typically used for dimensionality reduction and performance improvement (Leng et al., 2010). The features with high discrimination and low correlation will be selected and provided with high weights (Leng and Zhang, 2013). Therefore, how to find the discriminantive subspace is the key to solve this problem. Random projection is one of the effective methods to find the discriminantive subspace. In Leng et al. (2011), Leng et al. (2012), two-directional two-dimensional random projection was proposed to project high-dimensional data into a two-dimensional discriminantive subspace. The discrimination power analysis preserved more discriminative coefficients from dual-source space, which was constituted by two-dimensional discrete cosine transform (Leng et al., 2017). The other is that most of the current models treated EEG emotion recognition as a pure pattern classification task, which cared only about the recognition accuracy but paid few attention to underlying neural mechanisms related to emotion expression.

In the present work, we take the two above mentioned limitations into consideration and propose a Graph Adaptive Semi-supervised Discriminative Subspace Learning (GASDSL) model for cross-session EEG emotion recognition under the semi-supervised learning framework (Jiang et al., 2017). Graph is an effective data structure to characterize the sample correlations by defining a similarity matrix (Jin et al., 2022), based on which a lot of learning tasks can be performed such as clustering (Wang et al., 2022b), dimensionality reduction (Kalantar and Mohammadi, 2018), feature selection (Shang et al., 2022; Li et al., 2018) and semi-supervised learning (Li et al., 2022b). However, separately performing graph learning and emotional state estimation of unlabeled EEG samples ignore the underlying interaction between both stages. In GASDSL, such disadvantage is circumvented by unifying the subspace graph learning and graph-based recognition tasks together into a single objective function. To be specific, the updating process of the subspace projection matrix in GASDSL is mediated by the adaptive maximum entropy graph learning and semi-supervised subspace emotional state estimation. That is, the discriminative subspace learning, adaptive maximum graph learning and the emotional state prediction of the unlabeled samples are jointly optimized in GASDSL for better recognition performance.

When compared with the existing studies, the present work has the following contributions.

- We propose a unified model GASDSL to jointly complete both the graph adaptive discriminative subspace learning and semi-supervised EEG emotion recognition. The local manifold of both the labeled and unlabeled EEG data is explored by introducing the maximum entropy regularizer to adaptively determine the neighborhood size of each EEG sample.
- The discriminative subspace learning serves as the central role in our proposed GASDSL model, which is simultaneously mediated by the semi-supervised label prediction and adaptive graph learning processes. In other words, both the label

information (*i.e.*, the given and the predicted ones) and graph-based data structure information contribute to the discriminative subspace exploration.
- Besides the improved emotion recognition accuracy, we provide more analysis on the learned projection matrix from two aspects. One is that it shows excellent performance in inducing discriminative subspace. The other is that it offers us an automatic and quantitative method in identifying the critical EEG frequency bands and brain regions in emotion recognition.

The remainder of this paper is structured as follows. Section 2 introduces the detailed model formulation and optimization of GASDSL. Comparative studies on two emotional EEG datasets and the result analysis are provided in Section 3. Connections and differences between GASDSL and some related models are discussed in Section 4. Section 5 concludes this paper and points out the future work.

2. Method

2.1. Preliminary

In this paper, uppercase and lowercase letters are respectively used to denote matrices and vectors. For matrix $\mathbf{A} \in \mathbb{R}^{n\times m}$, $\mathbf{a}^i$ denotes its i-th row, $\mathbf{a}_j$ denotes its j-th column, and a_{ij} denotes its (i,j)-th element.

Generally, in semi-supervised EEG emotion recognition setting, the EEG dataset we are given consists of two subsets. one is the labeled subset, which has l labeled EEG samples $\mathbf{X}_l = [\mathbf{x}_1, \mathbf{x}_2, \ldots, \mathbf{x}_l] \in \mathbb{R}^{d\times l}$ and the associated label indicator matrix $\mathbf{Y}_l = [\mathbf{y}^1; \mathbf{y}^2; \ldots; \mathbf{y}^l] \in \mathbb{R}^{l\times c}$ is given. The other is the unlabeled subset, consisting of u unlabeled EEG samples $\mathbf{X}_u = [\mathbf{x}_1, \mathbf{x}_2, \ldots, \mathbf{x}_u] \in \mathbb{R}^{d\times u}$ and its label indicator matrix $\mathbf{Y}_u = [\mathbf{y}^1, \mathbf{y}^2, \ldots, \mathbf{y}^u] \in \mathbb{R}^{u\times c}$ is unknown. Here, d represents the EEG sample dimensionality and c represents the number of emotional states. The label indicator vector of the $i|_{i=1}^{l}$-th sample, *i.e.*, $\mathbf{y}^i \in \mathbb{R}^{1\times c}$, is defined as

$$y_{ij} = \begin{cases} 1, & \text{if sample } \mathbf{x}_i \text{ belongs to the } j \text{ -th state;} \\ 0, & \text{otherwise.} \end{cases} \tag{1}$$

To simplify the notations, we introduce an augmented label indicator matrix $\mathbf{F} = [\mathbf{F}_l; \mathbf{F}_u] \in \mathbb{R}^{n\times c}$, where $n = l + u, \mathbf{F}_l = \mathbf{Y}_l$ and $\mathbf{F}_u$ is the pseudo-label of the unlabeled EEG data. Our goal is to predict $\mathbf{F}_u$ given $\mathbf{X} = [\mathbf{X}_l, \mathbf{X}_u]$ and $\mathbf{Y}_l$.

2.2. GASDSL model formulation

In Fig. 2, we show the overall framework of our proposed GASDSL model, which consists of three components, *i.e.*, discriminative subspace projection, optimal maximum entropy graph learning and the emotion state estimation.

It it well known that according to the k-means clustering, we can obtain the predicted labels of the unlabeled EEG samples by iteratively updating the cluster centroids and assigning class labels to EEG samples. Its objective function is

$$\min_{\mathbf{F}\in \text{Ind}} \sum_{j=1}^{c} \sum_{\mathbf{x}_i \in \pi_j} \|\mathbf{x}_i - \mathbf{m}_j\|_2^2, \tag{2}$$

where $\mathbf{F} = [\mathbf{F}_l; \mathbf{F}_u] = [\mathbf{f}^1; \cdots; \mathbf{f}^l; \mathbf{f}^{l+1}; \cdots; \mathbf{f}^{l+u}] \in \mathbb{R}^{n\times c}$ is the label indicator matrix. To be specific, the i-th row of $\mathbf{F}$, *i.e.*, $\mathbf{f}^i \in \mathbb{R}^{1\times c}$, defines the emotional state of the i-th EEG sample $\mathbf{x}_i$. That is, $f_{ij} = 1$ if $\mathbf{x}_i$ belongs to the j-th emotional state and $f_{ij} = 0$ otherwise. In semi-supervised setting, $\mathbf{F}_l$ is given while $\mathbf{F}_u$ is to be estimated. $\mathbf{m}_j \in \mathbb{R}^d$ is the centroid of the j-th emotional state π_j. Mathematically, problem (2) can be rewritten as the following matrix form

$$\min_{\mathbf{F}\in \text{Ind}, \mathbf{M}} \|\mathbf{X} - \mathbf{M}\mathbf{F}^T\|_2^2, \tag{3}$$

where $\mathbf{M} = [\mathbf{m}_1, \mathbf{m}_2, \cdots, \mathbf{m}_c] \in \mathbb{R}^{d\times c}$ is the collection of all centroids. When $\mathbf{M}$ is fixed, we should annotate each EEG sample with the emotional state which its nearest centroid belongs to, leading to the updated indicator matrix $\mathbf{F}$. In turn, when $\mathbf{F}$ is fixed, $\mathbf{M}$ can be updated.

Generally, EEG data is high-dimensional and non-stationary, which inevitably includes noisy features and redundant components (Dadebayev et al., 2022). This phenomenon is common and challenging in EEG emotion recognition. An intuitive and effective way is to project EEG data into a low-dimensional subspace where the feature dimensionality is reduced while the discriminative ability is enhanced (Zhang et al., 2019). Assume that the discriminative subspace is induced by a projection matrix $\mathbf{W} \in \mathbb{R}^{d\times m}$, where m is the subspace dimensionality. Then, we have the following subspace semi-supervised clustering model

$$\min_{\mathbf{F}_l = \mathbf{Y}_l, \mathbf{F}_u \in \text{Ind}, \mathbf{M}, \mathbf{W}} \|\mathbf{W}^T\mathbf{X} - \mathbf{M}\mathbf{F}^T\|_2^2, \tag{4}$$

where $\mathbf{W}^T\mathbf{X} \in \mathbb{R}^{m\times n}$ is the projected subspace EEG data. To simplify the notations, we still use $\mathbf{M} \in \mathbb{R}^{m\times c}$ to represent the centroid matrix though its size is different from that in Eq. (3).

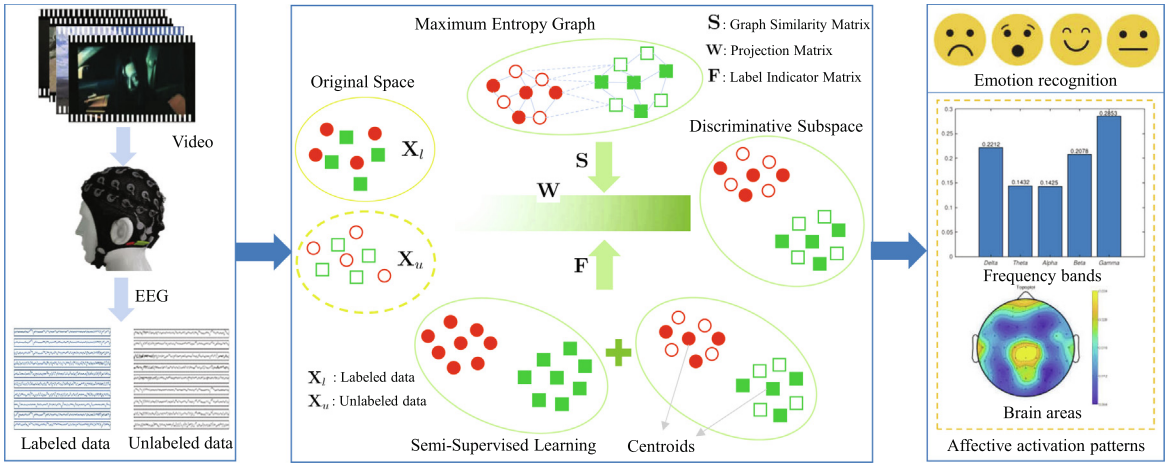

Fig. 2. The general framework of the proposed GASDSL model.

Below we describe how to find an optimal projection matrix $\mathbf{W}$ from the graph-based subspace learning perspective. We propose to explore the local structural information of EEG data within the structured graph learning framework (Nie et al., 2023; Peng et al., 2022a). In the low-dimensional subspace, we use $\mathbf{S} \in \mathbb{R}^{n\times n}$ to describe similarities of EEG samples in which $\mathbf{s}_{ij}$ characterizes the connectionship between the i-th and the j-th samples. To be specific, if the distance between $\mathbf{W}^T\mathbf{x}_i$ and $\mathbf{W}^T\mathbf{x}_j$ is small, they are more likely to have the same structure. Equivalently, the similarity $\mathbf{s}_{ij}$ should be large. Such property can be modeled by the following objective function

$$\begin{aligned} &\min_{\mathbf{W},\mathbf{S}} \sum_{i=1}^{n}\sum_{j=1}^{n} \|\mathbf{W}^T\mathbf{x}_i - \mathbf{W}^T\mathbf{x}_j\|_2^2 s_{ij}, \\ &s.t. s_{ij} \geqslant 0, \mathbf{s}^i\mathbf{1} = 1, \mathbf{W}^T\mathbf{S}_t\mathbf{W} = \mathbf{I}, \end{aligned} \tag{5}$$

where $\mathbf{S}_t = \mathbf{X}\mathbf{X}^T$ is the total data scatter matrix. The first constraint denotes the non-negativity of the similarity matrix. The second one enforces the summation of connection probabilities between $\mathbf{x}_i$ and all the other samples to be one. The third constraint ensures that the linear correlation between the subspace data is removed. Objective function (5) might have a trivial solution that only one element in $\mathbf{s}^i$ is one and the others are zeros Nie et al., 2014; Zheng et al., 2017). To avoid this dilemma, we introduce a maximum entropy regularizer to adaptively adjust the elements in $\mathbf{s}^i$ (Zhang et al., 2020b). Based on information theory, entropy measures the disorder of random variables and lager entropy represents higher disorder. For the n elements in $\mathbf{s}^i$, the entropy is $\phi(\mathbf{s}^i) = -\sum_{j=1}^{n} s_{ij}\log s_{ij}$. Since $s_{ij}|_{j=1}^{n}$ satisfies the probability constraint, $\phi(\mathbf{s}^i)$ reaches the minimum if only one element in $\mathbf{s}^i$ is one and the others are zeros, which represents the most informative distribution state of $\mathbf{s}^i$. However, this case is similar to the trivial solution of the objective function (5), which is also the most unstable state for assessing the probabilistic relationship. To avoid the performance loss which might be caused by the trivial solution, we incorporate the entropy maximization regularizer into objective function (5) to learn an adaptive similarity matrix to characterize local data informaiton. Then, we have

$$\begin{aligned} \min_{\mathbf{w},\mathbf{s}} \quad & \sum_{i=1}^{n}\sum_{j=1}^{n}\Big(\|\mathbf{W}^T\mathbf{x}_i - \mathbf{W}^T\mathbf{x}_j\|_2^2 s_{ij} + \beta s_{ij}\log s_{ij}\Big), \\ & s.t. s_{ij} \geqslant 0, \mathbf{s}^i\mathbf{1} = 1, \mathbf{W}^T\mathbf{S}_t\mathbf{W} = \mathbf{I}, \end{aligned} \tag{6}$$

Finally, by combining (4) and (6), we formulate the objective function of GASDSL as

$$\begin{aligned} &\min_{\mathbf{F},\mathbf{M},\mathbf{W},\mathbf{S}} \alpha\sum_{i,j=1}^{n}\Big(\|\mathbf{W}^T\mathbf{x}_i - \mathbf{W}^T\mathbf{x}_j\|_2^2 s_{ij} + \beta s_{ij}\log s_{ij}\Big) \\ &+\|\mathbf{W}^T\mathbf{X} - \mathbf{M}\mathbf{F}^T\|_2^2, s.t. \mathbf{F} = [\mathbf{F}_l; \mathbf{F}_u], \mathbf{F}_l = \mathbf{Y}_l, \\ &\mathbf{F}_u \in \mathrm{Ind}, s_{ij} \geqslant 0, \mathbf{s}^i\mathbf{1} = 1, \mathbf{W}^T\mathbf{S}_t\mathbf{W} = \mathbf{I}, \end{aligned} \tag{7}$$

where α and β denote two regularization parameters to balance the impacts of respective terms.

2.3. GASDSL model optimization

There are four variables $\mathbf{S}, \mathbf{F}_u, \mathbf{M}, \mathbf{W}$ in GASDSL objective function (7). Below we derive the updating rule to each of them. Specifically, we update one variable by fixing the three others.

■ Update $\mathbf{S}$. The corresponding objective function is

$$\begin{aligned} \min_{\mathbf{S}} \quad & \sum_{i=1}^{n}\sum_{j=1}^{n}\Big(\|\mathbf{W}^T\mathbf{x}_i - \mathbf{W}^T\mathbf{x}_j\|_2^2 s_{ij} + \beta s_{ij}\log s_{ij}\Big), \\ & s.t. s_{ij} \geqslant 0, \mathbf{s}^i\mathbf{1} = 1. \end{aligned} \tag{8}$$

Since the above problem can be decoupled for each $i = 1, 2, \cdots, n$, we propose to solve $\mathbf{S}$ in row-wise manner. For each i, we have the following objective function

$$\begin{aligned} \min_{\mathbf{s}^i} \quad & \sum_{j=1}^{n}\Big(\|\mathbf{W}^T\mathbf{x}_i - \mathbf{W}^T\mathbf{x}_j\|_2^2 s_{ij} + \beta s_{ij}\log s_{ij}\Big), \\ & s.t. \mathbf{s}^i \geqslant \mathbf{0}, \mathbf{s}^i\mathbf{1} = 1. \end{aligned} \tag{9}$$

To simplify the notations, we define $d_{ij} = \|\mathbf{W}^T\mathbf{x}_i - \mathbf{W}^T\mathbf{x}_j\|_2^2$ and then rewrite problem (9) as

$$\min_{\mathbf{s}^i \geqslant \mathbf{0}, \mathbf{s}^i\mathbf{1}=1} \sum_{j=1}^{n}\big(d_{ij}s_{ij} + \beta s_{ij}\log s_{ij}\big). \tag{10}$$

The corresponding Lagrangian function is

$$\mathscr{L}(s_{ij}, \theta) = \sum_{j=1}^{n}\big(d_{ij}s_{ij} + \beta s_{ij}\log s_{ij}\big) + \theta(\mathbf{s}^i\mathbf{1} - 1), \tag{11}$$

where θ is the Lagrange multiplier. By setting the derivative of (11) w.r.t. s_{ij} to zero, and combining the constraint $\sum_{j=1}^{n} s_{ij} = 1$, we obtain the updating rule of s_{ij} as

$$s_{ij} = \frac{\exp(\frac{-d_{ij}}{\beta})}{\sum_{j=1}^{n}\exp(\frac{-d_{ij}}{\beta})}. \tag{12}$$

Obviously, the above updating rule to s_{ij} definitely satisfies the non-negative constraint, *i.e.*, $\mathbf{s}^i \geqslant \mathbf{0}$.

■ Update $\mathbf{F}_u$. The sub-objective function related to $\mathbf{F}_u$ is

$$\begin{aligned} &\min_{\mathbf{F}} \|\mathbf{W}^T\mathbf{X} - \mathbf{M}\mathbf{F}^T\|_2^2, \\ &s.t. \quad \mathbf{F} = [\mathbf{F}_l; \mathbf{F}_u], \mathbf{F}_l = \mathbf{Y}_l, \mathbf{F}_u \in \mathrm{Ind}. \end{aligned} \tag{13}$$

Each row of $\mathbf{F}_u$ determines the emotional state of the i-th EEG sample. For each $i|_{i=l+1}^{n}$, we have

$$f_{ij} = \begin{cases} 1, & j = \arg\min_{k=1}^{c} \|\mathbf{W}^T\mathbf{x}_i - \mathbf{m}_k\|_2^2, \\ 0, & \text{otherwise}, \end{cases} \tag{14}$$

where $\mathbf{m}_k$ is the k-th column of the centroid matrix $\mathbf{M}$. Obviously, we should categorize the i-th sample into the class which its nearest subspace centroid belongs to.

■ Update $\mathbf{M}$. The sub-objective function regrading to variable $\mathbf{M}$ is

$$\min_{\mathbf{M}} \|\mathbf{W}^T\mathbf{X} - \mathbf{M}\mathbf{F}^T\|_2^2. \tag{15}$$

Taking the derivative of the above function w.r.t. $\mathbf{M}$ and setting it to zero, we obtain

$$\mathbf{M} = \mathbf{W}^T\mathbf{X}\mathbf{F}(\mathbf{F}^T\mathbf{F})^{-1}. \tag{16}$$

■ Update $\mathbf{W}$. The objective function related to $\mathbf{W}$ is

$$\begin{aligned} &\min_{\mathbf{W}^T\mathbf{S}_t\mathbf{W}=\mathbf{I}} \|\mathbf{W}^T\mathbf{X} - \mathbf{M}\mathbf{F}^T\|_2^2 \\ &+\alpha\sum_{i=1}^{n}\sum_{j=1}^{n}\|\mathbf{W}^T\mathbf{x}_i - \mathbf{W}^T\mathbf{x}_j\|_2^2 s_{ij}. \end{aligned} \tag{17}$$

By substituting $\mathbf{M}$ into the first term of the above equation, we obtain

$$\begin{aligned}
&\|\mathbf{W}^T\mathbf{X}-\mathbf{M}\mathbf{F}^T\|_2^2\\
&=\|\mathbf{W}^T\mathbf{X}-\mathbf{W}^T\mathbf{X}\mathbf{F}(\mathbf{F}^T\mathbf{F})^{-1}\mathbf{F}^T\|_2^2\\
&=\mathrm{Tr}(\mathbf{X}^T\mathbf{W}\mathbf{W}^T\mathbf{X}-\mathbf{X}^T\mathbf{W}\mathbf{W}^T\mathbf{X}\mathbf{F}(\mathbf{F}^T\mathbf{F})^{-1}\mathbf{F}^T)\\
&=\mathrm{Tr}(\mathbf{W}^T(\mathbf{X}\mathbf{X}^T-\mathbf{X}\mathbf{F}(\mathbf{F}^T\mathbf{F})^{-1}\mathbf{F}^T\mathbf{X}^T)\mathbf{W})\\
&=\mathrm{Tr}(\mathbf{W}^T(\mathbf{S}_t-\mathbf{S}_b)\mathbf{W})=\mathrm{Tr}(\mathbf{W}^T\mathbf{S}_w\mathbf{W}),
\end{aligned}\tag{18}$$

where $\mathbf{S}_b$ represents the inter-class data scatter matrix and $\mathbf{S}_w$ denotes the intra-class data scatter matrix. It is easy to find that

$$\mathbf{S}_w=\mathbf{X}\mathbf{X}^T-\mathbf{X}\mathbf{F}(\mathbf{F}^T\mathbf{F})^{-1}\mathbf{F}^T\mathbf{X}^T.\tag{19}$$

Then, problem (17) can be rewritten as

$$\min_{\mathbf{W}^T\mathbf{S}_t\mathbf{W}=\mathbf{I}}\ \mathrm{Tr}(\mathbf{W}^T\mathbf{S}_w\mathbf{W})+\alpha\mathrm{Tr}(\mathbf{W}^T\mathbf{X}\mathbf{L}\mathbf{X}^T\mathbf{W}),\tag{20}$$

where $\mathbf{L}=\mathbf{D}-\mathbf{S}$ is the graph Laplacian matrix, $\mathbf{D}$ is the diagonal matrix and its i-th diagonal element is defined as $d_{ii}=\sum_j s_{ij}$. The Lagrangian function of problem (20) is

$$\begin{aligned}
\mathscr{L}(\mathbf{W},\mathbf{\Lambda})=\ &\mathrm{Tr}(\mathbf{W}^T(\mathbf{S}_w+\alpha\mathbf{X}\mathbf{L}\mathbf{X}^T)\mathbf{W})\\
&-\mathrm{Tr}(\mathbf{\Lambda}(\mathbf{W}^T\mathbf{S}_t\mathbf{W}-\mathbf{I})),
\end{aligned}\tag{21}$$

where $\mathbf{\Lambda}$ is the Lagrange multiplier in matrix form. By taking the derivative of $\mathscr{L}(\mathbf{W})$ w.r.t. $\mathbf{W}$, and setting it to zero, we have

$$(\mathbf{S}_w+\alpha\mathbf{X}\mathbf{L}\mathbf{X}^T)\mathbf{W}-\mathbf{S}_t\mathbf{W}\mathbf{\Lambda}=\mathbf{0}.\tag{22}$$

Then, the optimal solution $\mathbf{W}^*$ to problem (21) can be formed by stacking the m eigenvectors of $\mathbf{S}_t^{-1}(\mathbf{S}_w+\alpha\mathbf{X}\mathbf{L}\mathbf{X}^T)$ corresponding to its m smallest eigenvalues. To guarantee that $\mathbf{S}_t$ is invertible, it is assumed that the null space of the EEG data matrix $\mathbf{X}$ has been removed.

We summarize the above optimization steps to GASDSL objective function in Algorithm 1.

Algorithm 1 The optimization to GASDSL objective function

Input: Labeled EEG data $\mathbf{X}_l\in\mathbb{R}^{d\times l}$ and the corresponding label matrix $\mathbf{Y}_l\in\mathbb{R}^{l\times c}$, unlabeled EEG data $\mathbf{X}_u\in\mathbb{R}^{d\times u}$, subspace dimensionality m, parameters α and β;
Output: The estimated label indicator matrix $\mathbf{F}_u\in\mathbb{R}^{u\times c}$.
1: Initialize the projection matrix $\mathbf{W}$ by principal component analysis;
2: Initialize the centroid matrix $\mathbf{M}$ by $\mathbf{W}^T\mathbf{X}_l$;
3: Initialize the graph similarity matrix $\mathbf{S}$ by solving problem $\min_{\forall i,\mathbf{s}^i\geq\mathbf{0},\mathbf{s}^i\mathbf{1}=1}\sum_{i=1}^n\sum_{j=1}^n\|\mathbf{x}_i-\mathbf{x}_j\|_2^2 s_{ij}+\beta s_{ij}\log s_{ij}$;
4: **while** not converged **do**
5: Update $\mathbf{F}_u$ row-wisely by Eq. (14);
6: Update $\mathbf{M}$ by Eq. (16);
7: Update diagonal matrix $\mathbf{D}$ with $d_{ii}=\sum_{j=1}^n s_{ij}$;
8: Update $\mathbf{S}_w$ by Eq. (19);
9: Update $\mathbf{W}$ by the m eigenvectors of $\mathbf{S}_t^{-1}(\mathbf{S}_w+\alpha\mathbf{X}\mathbf{L}\mathbf{X}^T)$ corresponding to the first m smallest eigenvalues;
10: Update $\mathbf{S}$ row-wisely by Eq. (12);
11: **end while**

2.4. Complexity and convergence analysis

Below we provide the computational complexity analysis of our optimization algorithm to GASDSL objective function by the big $\mathcal{O}$ notation. We need $\mathcal{O}(umd)$ complexity to obtain $\mathbf{F}_u$. The updating of $\mathbf{M}$ needs $\mathcal{O}(nmd)$ time. When updating $\mathbf{W}$, the complexity is $\mathcal{O}(d^3+n^2d+nd^2)$. For each $i\in[1,n]$, we need $\mathcal{O}(dm)$ time to update $\mathbf{s}^i$. Therefore, we need $\mathcal{O}(nmd)$ to obtain $\mathbf{S}$. Assuming that the number of iterations is t, the computational complexity of optimizing GASDSL objective function is $\mathcal{O}(t(umd+nmd+d^3+n^2d+nd^2))$. Considering that the usual case is $n\approx u>d>m\gg c$ in semi-supervised emotion recognition tasks, the overall complexity of GASDSL is $\mathcal{O}(tn^2d)$.

On the convergence property of GASDSL, we provide the analysis below. The convergence of updating the label indicator matrix $\mathbf{F}_u$ and centroid matrix $\mathbf{M}$ has been well studied in k-means clustering which definitely can be guaranteed. When updating the graph similarity matrix row-wisely, each row of $\mathbf{S}$ has analytical solution as in Eq. (12). Similarly, the solution to projection matrix $\mathbf{W}$ is obtained by generalized eigen-decomposition operation. Therefore, Algorithm 1 is expected to have desirable convergence property.

3. Experiments

In the section, comparative studies are performed to evaluate the effectiveness of GASDSL. We are interested in the following three aspects, the emotion recognition performance, the discriminative ability of the learned subspace, and the identified EEG spatial-frequency patterns in emotion recognition.

3.1. Data description

We perform experiments on two benchmark emotional EEG datasets, *i.e.*, SEED-IV (Zheng et al., 2018) and SEED-V (Liu et al., 2022), which are provided by Shanghai Jiao Tong University and publicly available.

In SEED-IV, 15 healthy subjects were recruited for the EEG data collection experiment and each subject participated the experiment at three different times, corresponding to the three sessions. Therefore, there are total 45 sessions. 72 video clips were carefully chosen to elicit four different types of emotional states, *i.e.*, *sad*, *fear*, *happy* and *neutral*. In each session, 24 video clips were displayed, among which six clips correspond to one emotional state. During each subject watching the video clips, EEG data was collected by the ESI NeuroScan system with a 62-channel electrode cap according to the standard international 10–20 placement.

In preprocessing stage, EEG data was down-sampled from 1000 Hz to 200 Hz and then band-pass filtered to 1–50 Hz for artifact removal. We adopted the Differential Entropy (DE) in the following experiments (Zhang et al., 2020a), which were extracted from the five frequency bands, *i.e.*, *Delta* (1–3 Hz), *Theta* (4–7 Hz), *Alpha* (8–13 Hz), *Beta* (14–30 Hz) and *Gamma* (31–50 Hz). There are five frequency bands and each one has 62 values (corresponding to the 62 EEG channels); therefore, the feature dimensionality of EEG sample vectors is 310. Due to slightly different durations of video clips in each session, we have respectively 851, 832 and 822 EEG samples in the three sessions.

The data collection paradigm of SEED-V is similar to that in SEED-IV; however, there are five emotional states, *i.e.*, *fear*, *sad*, *neutral*, *happy* and *disgust*. There are 20 subjects participated in the experiment of EEG collection, and the EEG data of 16 subjects were made publicly available. Similarly, each subject has three different sessions, each of which has 15 trials and three trials correspond to one emotional state. We also extract the DE feature from the above mentioned five frequency bands and then form EEG sample vectors with dimensionality 310. There are total 681, 541 and 601 samples in the three sessions, respectively. The general properties of the two datasets are shown in Table 1.

Table 1
Summary of the emotional EEG datasets.

Item	SEED-IV	SEED-V
# subject	15	16
feature	differential entropy (DE)	differential entropy (DE)
# electrode	62	62
frequency bands	*Delta*, *Theta*, *Alpha*, *Beta*, *Gamma*	*Delta*, *Theta*, *Alpha*, *Beta*, *Gamma*
emotional states	*sad*, *fear*, *happy*, *neutral*	*fear*, *sad*, *neutral*, *happy*, *disgust*

3.2. Experimental settings

In the following experiments, we compare our proposed GASDSL model with some semi-supervised models, including semi-supervised Projected Clustering with Adaptive Neighbors (sPCAN) (Nie et al., 2014), semi-supervised Support Vector Machine (sSVM), semi-supervised Linear Square Regression (sLSR) with linear kernel, Rescaled Linear Square Regression (RLSR) (Chen et al., 2017; Chen et al., 2020), semi-supervised version of the Unified Framework of Dimensionality Reduction (sUFDR) (Wu et al., 2020), semi-supervised label propagation by optimal Maximum Entropy Graph learning (sMEG) (Nie et al., 2023; Zhong et al., 2021), sparse discriminative semi-supervised feature selection (SDSSFS) (Wang et al., 2022a) and semi-supervised sparse low-rank regression (S^3LRR) (Peng et al., 2022c). In sPCAN, we first learn an optimal graph based on PCAN and then perform label propagation on it to predict the emotional states of unlabeled EEG samples. In RLSR, an explicit feature importance descriptor is introduced into the semi-supervised LSR model to distinguish the different contributions of features in classifying emotional states. sLSR is a degenerated version of RLSR without taking the adaptive feature auto-weighting into consideration. sUFDR iteratively performs subspace *k*means clustering and semi-supervised dimensionality reduction. The objective of sMEG is formed by replacing the ℓ_2-norm regularization on the graph similarity matrix in (Peng et al., 2022a) with the graph regularization. SDSSFS utilizes the idea of enlarging the distance between classes and simultaneously estimates the label information of unlabeled samples by the learned regression coefficients and ε-dragging matrix. S^3LRR improved the LSR by replacing the projection matrix with the multiplication of two factor matrices, which realized the unification of discriminative subspace learning and semi-supervised emotion state recognition.

In both SEED-IV and SEED-V, each subject has multiple sessions. Therefore, we propose to perform subject-dependent cross-session EEG emotion recognition tasks including the 'session1→session2' task, 'session1→session3' task, and 'session2→session3' task. Taking the first one as an example, it means that EEG samples from the first session are fully labeled and those from the second session as unlabeled. Considering that there might be inter-session EEG data variabilities, we performed a two-step preprocessing prior to model training. One is mapping the values of each feature dimension into [0, 1] to reduce the scale mismatch. The other is the data centralization. The parameters involved in respective models are tuned from $\{2^{-10}, 2^{-9}, \cdots, 2^{10}\}$. The range of regularization parameters α and β in GASDSL is $\{2^{-5}, 2^{-4}, \cdots, 2^{15}\}$. The subspace dimensionality parameter m in GASDSL and sMEG are tuned from {10, 20, 30, 50, 70, 100, 150, 200}. The maximal iteration number is set as 50.

3.3. Results and analysis

The accuracies of the three cross-session emotion recognition tasks are respectively shown in Tables 2–7, where boldface number is used to highlight the highest one in each case. s1, s2, and so on represent the indices of subjects. m1, m2, and so on respectively correspond to sPCAN, sSVM, sLSR, RLSR, sUFDR, sMEG, SDSSFS, S^3LRR, GASDSL. These results provide us with the following rationalities.

- Compared with the other models, GASDSL achieved the best average accuracies in all emotion recognition tasks. On SEED-IV, its average accuracies of the three cross-session emotion recognition tasks are 77.08%, 78.80%, and 81.88% and GASDSL respectively improved the performance by 3.06%, 4.06%, and 4.59% when compared with the second-best model. Meanwhile, GASDSL achieved the average accuracies on the SEED-V dataset are 81.57%, 81.57% and 82.03%, which have 3.01%-5.80% improvements in comparison with the runner-up model. Therefore, We conclude that unifying the graph adaptive discriminative subspace learning, and semi-supervised subspace emotional state estimation in a single optimization framework is beneficial for achieving better performance in EEG emotion recognition.
- Based on the experimental results, sPCAN demonstrated the worst performance among these models. To be specific, it respectively obtained the average accuracies of 55.85%, 57.66%, and 58.86% on SEED-IV and 46.49%, 44.17% and 48.75% on SEED-V. The reason accounting for such result might be from the two defects in sPCAN. One is that the structured graph learning process is totally unsupervised, which did not take full advantage of the available data label information. The other is that its two-stage strategy completes the graph learning and label propagation in sequential manner, meaning that the underlying connections between them are ignored. Though sSVM had sightly better performance than sPCAN, its overall performance is still unsatisfactory. Probably, the linear kernel in it is of limited ability in capturing the semantic connections of EEG samples.
- By introducing a feature self-weighting variable into the semi-supervised regression, RLSR is endowed with the ability of adaptively learning the different contributions of EEG features in classifying the emotional states. As a result, RLSR respectively outperforms sLSR by 2.62%, 2.48%, and 3.01% on SEED-IV and 2.05%, 3.22% and 1.75% on SEED-V. This is consistent with our intuitive understanding that emotion expression might be correlated more to some specific EEG frequency bands (channels), from which EEG features were extracted. In the subsequent section, we will show how to quantitatively measure the importance of them.
- By pair-wisely comparing their results, GASDSL outperforms sMEG by approximately 3.06%-8.48%. According to our understanding, the projection matrix induced subspace acts as different roles in these two models. In sMEG, the subspace is mainly explored for structured graph learning based on which the emotional states of unlabeled samples are estimated by label propagation. Differently, the discriminative subspace learning in GASDSL serves as the central position which connects the graph construction and emotional state prediction from both sides. As a semi-supervised learning model, GASDSL can perform prediction on unseen EEG samples besides the given unlabeled samples. However, the graph-based emotional state propagation in sMEG is a transductive process which has no out-of-sample extension ability.

In order to show the performance of the compared models more explicitly, the average emotion recognition accuracies of them are provided in Fig. 3, which employs the line charts to more explicitly show the performance differences among these models. For example, in Fig. 3a), the blue, red and yellow lines respectively represent the 'session1→session2', 'session1→session3' and 'session2→session3' tasks on the SEED-IV dataset. The knots in each line represent the recognition accuracies of different models, from which we can easily identify the performance trends of these models. Besides, we find that these models exhibit better performance in the 'session2→session3' task than the other two ones. For the

Table 2
Emotion recognition accuracies (%) of 'session1→session2' on the SEED-IV dataset.

Subject	m1	m2	m3	m4	m5	m6	m7	m8	m9
s1	52.76	39.42	57.09	55.65	76.44	75.48	53.61	48.32	**80.17**
s2	76.32	78.97	91.23	89.18	80.05	85.82	89.66	**96.88**	89.06
s3	51.68	53.37	60.10	69.71	71.51	72.36	67.79	**80.29**	77.40
s4	37.50	31.13	63.22	68.39	**82.09**	70.55	70.55	70.55	76.32
s5	40.63	47.24	59.50	67.67	69.11	**72.00**	68.39	70.07	69.35
s6	50.12	48.32	69.83	71.03	72.24	69.35	70.55	72.84	**77.16**
s7	66.95	68.99	82.93	80.77	71.15	74.88	80.77	**91.59**	79.33
s8	66.59	70.91	68.87	69.95	78.97	76.32	70.43	71.75	**80.89**
s9	57.81	60.82	67.67	78.73	72.96	75.36	79.09	62.98	**80.77**
s10	52.64	58.17	46.75	53.85	**74.16**	68.15	55.89	64.18	72.48
s11	50.36	53.37	50.00	52.04	63.22	67.43	52.04	64.66	**68.75**
s12	44.23	40.26	60.34	53.13	60.34	58.77	**70.67**	69.83	60.58
s13	42.79	54.81	58.05	68.63	63.94	68.27	69.59	**70.31**	69.79
s14	67.79	68.75	79.33	76.92	77.88	78.13	74.76	76.92	**79.63**
s15	79.57	81.37	88.58	87.14	94.95	**97.36**	**97.36**	94.23	94.47
Avg.	55.85	57.06	66.90	69.52	73.93	74.02	71.41	73.69	**77.08**

Table 3
Emotion recognition accuracies (%) of 'session1→session3' on the SEED-IV dataset.

Subject	m1	m2	m3	m4	m5	m6	m7	m8	m9
s1	54.99	50.12	64.72	70.68	59.12	75.67	70.19	**78.71**	75.84
s2	75.43	71.05	84.55	89.29	85.04	**92.70**	85.64	84.91	87.23
s3	45.13	57.66	48.42	48.78	62.77	75.43	45.50	59.61	**83.45**
s4	56.69	57.66	71.05	71.17	72.75	79.44	79.32	72.14	**79.83**
s5	43.07	43.07	52.55	58.39	64.72	64.11	**74.57**	70.07	73.84
s6	74.70	60.46	80.17	83.45	76.03	81.14	83.58	**84.91**	76.64
s7	66.55	57.91	86.98	88.44	81.63	86.13	84.79	86.74	**88.81**
s8	65.33	71.41	78.22	80.78	71.65	80.41	**81.87**	72.14	79.56
s9	47.57	48.30	61.68	62.77	74.09	69.10	62.77	51.22	**75.43**
s10	60.83	61.31	45.26	49.64	**75.30**	63.87	49.64	66.30	73.48
s11	54.99	60.71	76.28	71.17	79.56	65.94	70.68	**84.06**	78.59
s12	40.63	33.09	65.82	65.45	54.14	57.54	66.79	**68.13**	65.94
s13	55.84	61.80	54.87	62.41	73.11	64.11	61.31	55.23	**74.09**
s14	61.56	55.84	77.49	82.85	76.89	77.74	82.73	**84.91**	83.73
s15	61.68	80.78	85.52	85.40	82.73	87.71	85.40	**87.83**	85.52
Avg.	57.66	58.08	68.90	71.38	72.64	74.74	72.32	73.80	**78.80**

Table 4
Emotion recognition accuracies (%) of 'session2→session3' on the SEED-IV dataset.

Subject	m1	m2	m3	m4	m5	m6	m7	m8	m9
s1	53.41	56.69	61.44	62.65	64.96	74.09	61.68	63.87	**75.30**
s2	81.75	79.20	85.40	83.21	85.52	**89.54**	86.74	89.42	86.37
s3	43.31	67.88	63.75	67.27	68.49	75.43	68.98	76.03	**82.73**
s4	54.14	67.64	82.48	80.17	77.01	76.03	**89.54**	85.04	84.43
s5	57.66	64.23	76.64	72.87	66.42	71.41	77.98	**80.54**	77.01
s6	60.22	65.57	76.64	83.70	77.01	84.79	**93.55**	88.69	85.04
s7	82.00	85.04	84.31	88.56	85.89	87.83	89.78	87.96	**92.94**
s8	55.96	64.48	76.52	**82.97**	71.29	76.52	80.41	64.96	81.75
s9	53.04	59.25	47.45	61.80	**80.29**	73.60	58.39	66.79	75.43
s10	45.01	53.16	72.87	78.35	80.78	79.68	78.35	70.80	**85.52**
s11	47.81	52.55	52.68	59.49	72.02	55.84	73.60	45.38	**78.59**
s12	37.47	42.09	67.88	63.63	51.95	63.02	70.32	**75.43**	68.98
s13	57.18	41.85	56.45	64.48	73.36	73.72	62.17	57.79	**76.16**
s14	68.61	71.53	88.44	87.10	87.71	87.47	87.10	**95.01**	90.75
s15	85.28	85.40	88.08	89.90	83.94	90.39	**93.07**	92.09	87.23
Avg.	58.86	63.77	72.07	75.08	75.11	77.29	78.11	75.99	**81.88**

SEED-V dataset, similar trends are found in Fig. 3b) that GASDSL is better than the others. What is the difference is that these models obtained similar and better performance in the 'session1→session2' and 'session2→session3' tasks but worse performance in the 'session1→session3' task. In order to verify that our proposed model is significantly different from other models, we performed the one-way analysis of variance (ANOVA) on the experimental results obtained by GASDSL and the other compared models. The purpose of using ANOVA is to evaluate whether the recognition accuracy of the models are significantly different. The null hypothesis of ANOVA is that the means of these result groups corresponding to different models are equal. Table 8 shows the p-values returned by the ANOVA function. P-value is an index to measure the difference between two groups. When the p-value approaches 0, it indicates that the null hypothesis is rejected. P-value less than 0.05 shows the significant difference between the two models, while p-value less than 0.01 indicates extremely significant difference. Therefore, we conclude that GASDSL significantly

Table 5
Emotion recognition accuracies (%) of 'session1→session2' on the SEED-V dataset.

Subject	m1	m2	m3	m4	m5	m6	m7	m8	m9
s1	47.69	72.46	87.80	84.29	77.82	82.26	87.80	87.80	**88.72**
s2	46.21	40.11	62.48	62.29	76.52	77.08	70.98	75.60	**82.62**
s3	53.97	39.00	51.02	59.52	70.24	67.65	61.37	68.95	**80.04**
s4	49.72	57.30	90.20	90.57	80.96	85.21	**93.90**	85.77	88.35
s5	53.97	47.32	74.49	**79.67**	68.95	70.24	79.30	76.16	76.52
s6	40.85	54.34	68.95	72.64	79.30	75.23	75.97	72.64	**82.26**
s7	49.91	49.35	81.59	81.59	76.16	75.79	**82.44**	81.89	81.70
s8	44.36	60.07	62.66	74.68	78.00	69.69	80.59	78.19	**83.18**
s9	44.55	50.09	69.32	72.46	74.86	80.22	79.85	81.15	**87.99**
s10	43.81	46.40	54.90	58.23	60.81	68.13	60.44	67.10	**68.58**
s11	52.31	63.77	66.73	71.90	63.22	76.21	75.79	66.91	**76.52**
s12	41.77	49.54	77.63	81.15	76.89	66.54	81.52	**82.99**	76.89
s13	42.33	66.36	81.15	84.66	81.70	83.92	89.65	**90.76**	90.39
s14	43.25	36.41	76.71	73.01	73.57	77.08	**88.17**	78.56	77.45
s15	48.06	56.93	52.68	48.98	80.59	69.69	56.56	79.30	**84.10**
s16	41.04	53.79	**90.94**	86.51	68.21	72.83	**90.94**	82.07	79.85
Avg.	46.49	52.70	71.83	73.88	74.24	74.86	78.45	78.49	**81.57**

Table 6
Emotion recognition accuracies (%) of 'session1→session3' on the SEED-V dataset.

Subject	m1	m2	m3	m4	m5	m6	m7	m8	m9
s1	49.92	73.71	69.88	70.72	65.89	**87.35**	75.04	73.54	80.03
s2	37.60	55.74	60.73	64.23	66.06	57.74	68.05	67.22	**77.54**
s3	40.10	56.07	56.91	69.55	72.38	72.38	78.20	75.71	**84.69**
s4	49.25	67.22	89.52	89.52	86.86	83.03	**93.18**	90.02	90.35
s5	46.42	51.91	57.40	65.56	74.21	74.38	74.88	76.04	**81.86**
s6	41.43	45.76	45.26	48.09	73.54	42.26	52.58	57.40	**77.04**
s7	38.77	54.58	75.87	79.53	74.04	73.38	91.18	**91.35**	86.86
s8	58.57	50.08	73.04	68.89	75.54	60.73	67.89	76.54	**84.19**
s9	44.09	72.71	80.70	76.37	79.03	**92.85**	91.01	92.18	85.86
s10	47.09	38.44	46.92	46.59	58.23	55.41	54.24	50.58	**70.38**
s11	43.43	58.07	73.04	75.71	73.21	79.03	89.85	**93.84**	84.86
s12	38.94	57.40	68.89	79.87	69.72	78.87	**92.85**	89.02	83.69
s13	37.27	70.72	71.55	72.21	77.04	80.37	77.04	**92.85**	89.85
s14	44.09	53.24	55.57	65.72	58.40	**81.20**	64.89	64.56	67.89
s15	43.93	40.27	44.09	43.09	68.22	64.39	54.74	60.23	**72.88**
s16	45.76	49.08	61.73	66.89	75.71	70.05	68.55	61.23	**87.19**
Avg.	44.17	55.94	64.44	67.66	71.75	72.09	74.64	75.77	**81.57**

Table 7
Emotion recognition accuracies (%) of 'session2→session3' on the SEED-V dataset.

Subject	m1	m2	m3	m4	m5	m6	m7	m8	m9
s1	50.92	62.06	89.35	89.52	68.39	91.68	**96.51**	**96.51**	79.37
s2	45.92	58.07	82.20	80.53	70.55	74.38	89.35	**94.68**	71.05
s3	42.60	51.08	69.72	64.56	76.54	74.88	75.54	75.04	**84.53**
s4	67.72	65.39	70.38	79.20	84.86	86.52	85.36	80.87	**90.35**
s5	49.42	49.75	56.24	65.89	79.20	67.22	66.56	64.73	**79.70**
s6	40.77	48.92	64.23	65.56	71.55	65.39	68.89	72.55	**82.03**
s7	44.43	47.25	80.37	95.17	76.21	80.53	**97.84**	93.51	86.36
s8	49.92	50.75	78.04	73.04	82.03	67.89	84.86	**92.85**	86.86
s9	51.91	51.08	85.36	80.37	83.36	**94.34**	88.35	90.52	88.85
s10	39.60	59.73	37.60	44.59	63.89	65.56	47.75	47.75	**73.71**
s11	58.57	52.91	80.53	75.21	71.88	62.40	79.37	77.54	**82.70**
s12	47.25	64.89	83.86	83.36	69.05	76.87	88.35	**91.51**	78.54
s13	44.09	62.56	70.72	82.86	80.87	84.36	84.36	86.36	**88.85**
s14	43.59	38.60	47.42	47.75	63.06	54.08	56.41	58.07	**71.55**
s15	51.41	58.07	63.73	60.90	76.71	80.70	72.21	65.72	**82.03**
s16	51.91	59.40	70.88	70.05	76.54	72.71	71.15	76.04	**86.02**
Avg.	48.75	55.03	70.66	72.41	74.67	74.97	78.30	79.02	**82.03**

outperforms all the other models in emotion recognition based on the results in Table 8.

In addition to the recognition accuracy, we show the confusion matrices of GASDSL on SEED-IV and SEED-V in Fig. 4, from which we know the recognition accuracy of GASDSL for each emotional state. In confusion matrices, different depth of the color indicates different values. The darker the color, the larger the value. Taking SEED-IV for example, the recognition rates of the four emotional states *sad*, *fear*, *happy* and *neutral*, by GASDSL are 79.44%, 70.10%, 72.94% and 88.85%, respectively. Obviously, *neutral* is the state with the highest recognition rate; therefore, the corresponding block has the darkest color. In addition, we know that 5.12%, 3.07%, and 2.96% of the *neutral* EEG samples were respectively misclassified as the *sad*, *fear*, and *happy* states.

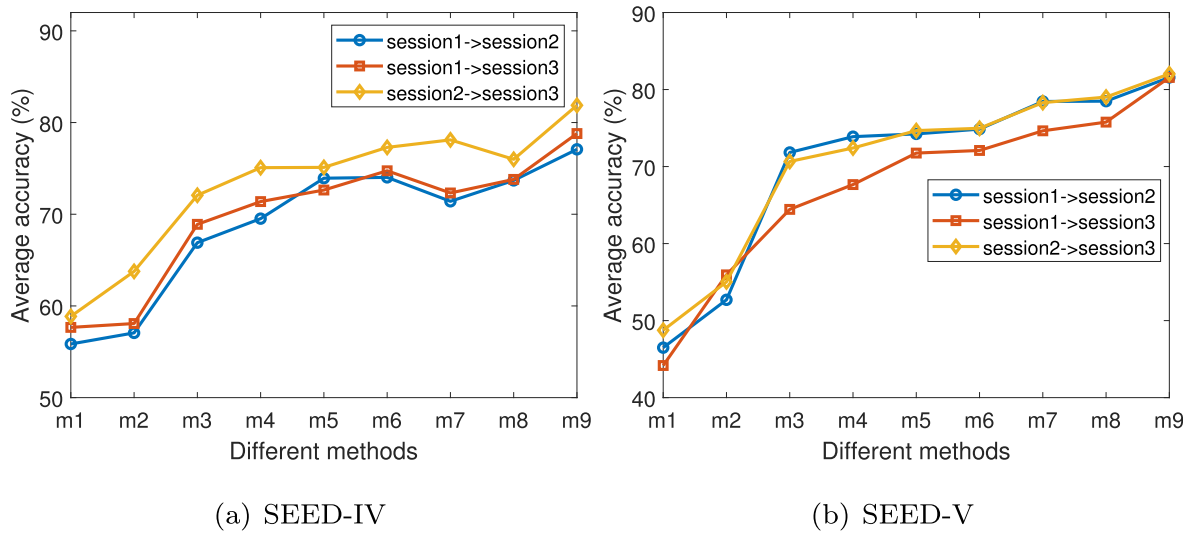

Fig. 3. Average emotion recognition accuracies of different models (%) represented by curves.

Table 8
The analysis of the variance(ANOVA) between GASDSL and the other models (**p-value < 0.01, *p-value < 0.05).

ANOVA	SEED-IV	SEED-V
m1	2.23e-16**	2.56e-48**
m2	1.92e-13**	3.49e-30**
m3	3.05e-05**	4.55e-08**
m4	8.18e-04**	1.72e-06**
m5	0.002325**	1.21e-08**
m6	0.002725**	2.16e-05**
m7	0.015448*	0.004296**
m8	0.032722*	0.018284*

3.4. Insights into the GASDSL model learning

3.4.1. Discriminative subspace learning

In GASDSL, the discriminative subspace learning is mediated by the graph learning and the pseudo-label estimation of unlabeled EEG samples. Mathematically, as shown by Eq. (20), it simultaneously minimizes the within-class data scatter (*i.e.*, the between-class scatter is accordingly maximized since the total scatter is fixed) and the discriminative information depicted by the learned graph. This section investigates the discriminative ability of the learned subspace by comparing GASDSL with sPCAN and sUFDR on both synthetic data and real EEG data.

First, we explore a toy example to verify the ability of GASDSL in dealing with non-Gaussian distributed data. The synthetic dataset is generated randomly and contains two classes of data points, consisting a labeled subset and an unlabeled subset. The dimension of each data point is two. We first add Gaussian noises on this dataset and then different dimensionality reduction methods are used to project it onto a 2D space. As shown in Fig. 5, all the three models perform well on this dataset when the noise variance is one and the number of noisy dimensions is 10. However, when the noise variance is enlarged to eight and the number of noisy dimensions is 100, the separability of datasets achieved by GASDSL significantly outperforms the other two models, as shown in Fig. 6.

Second, an example case (subject1: session1→session2) from the SEED-IV dataset is used to visualize the learned subspaces. In Fig. 7, the red, blue, green and yellow data points indicate the EEG samples respectively belonging to the *neutral*, *sad*, *fear* and *happy* states. It is obvious that in Fig. 7d), the samples from differen classes are almost perfectly separated, indicating the effectiveness of GASDSL in discriminative subspace learning.

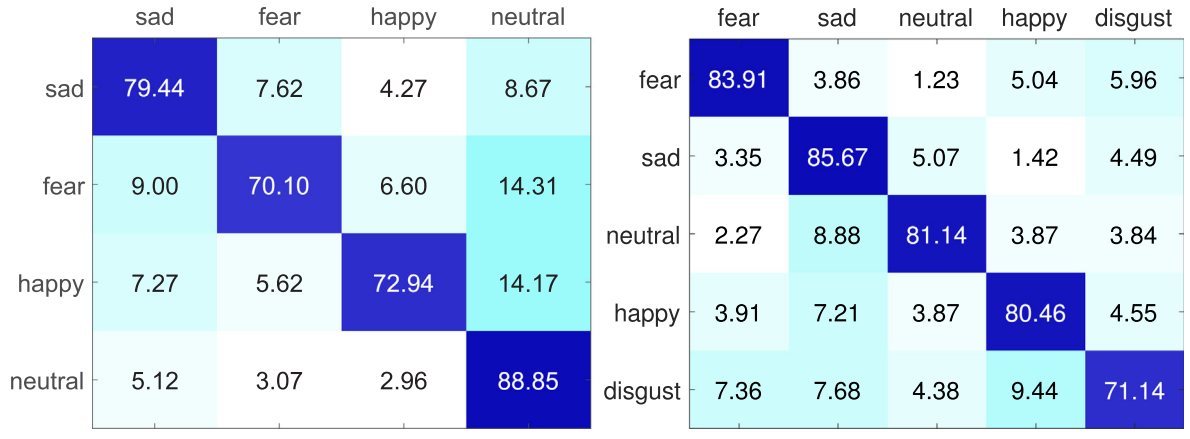

Fig. 4. Recognition accuracies (%) of GASDSL represented by confusion matrices.

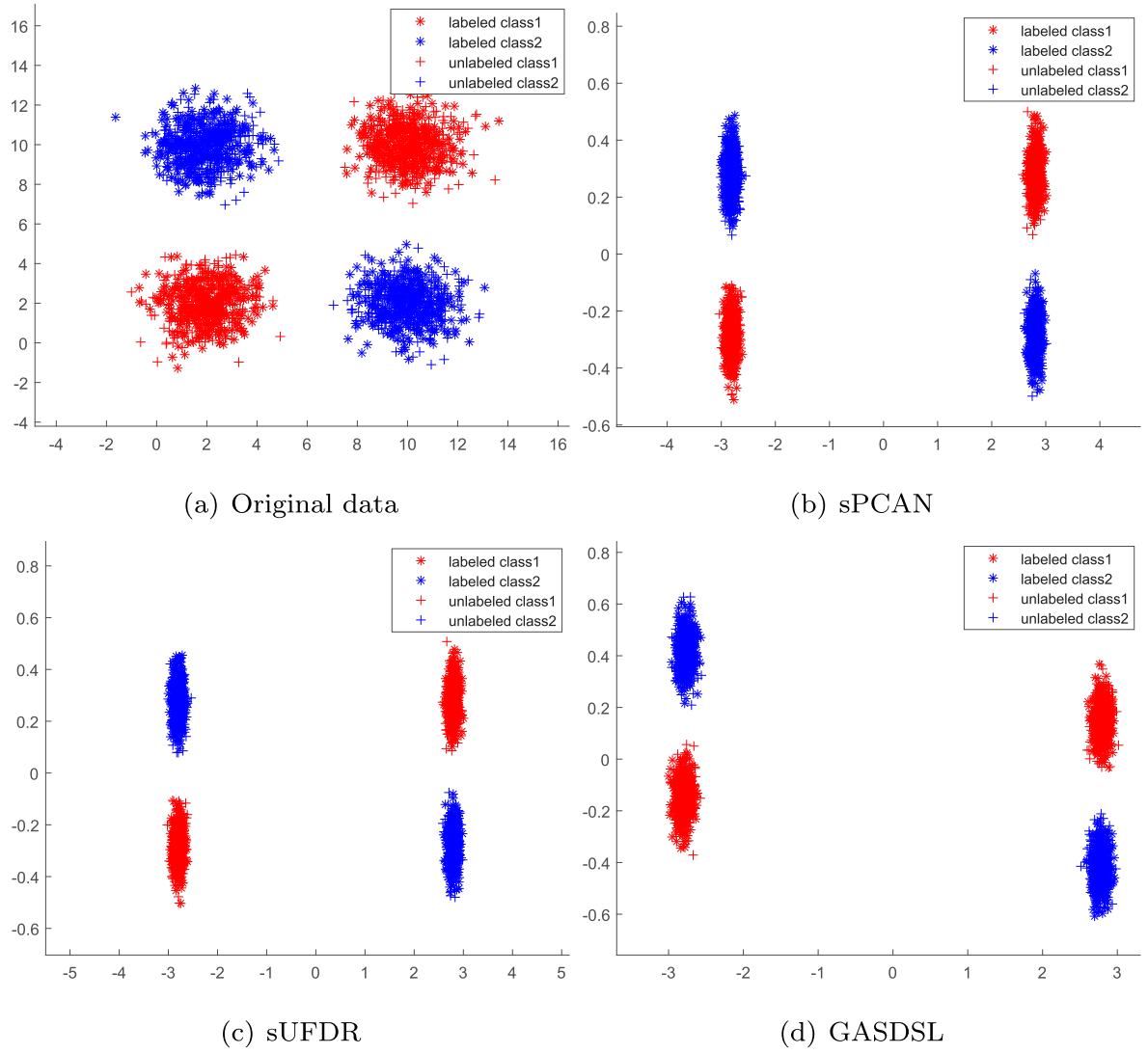

Fig. 5. Subspaces learning on a synthetic dataset with moderate noises.

3.4.2. Graph similarity learning

According to the graph theory, a desirable graph should properly establish connections for within-class samples but remove connections for between-class samples to enhance its discriminative ability. In GASDSL, the graph learning process is coupled with the other components of discriminative subspace learning and the pseudo-label estimation. Therefore, the maximal entropy graph learning is guided by the discriminative information consisting of given labels and estimated pseudo ones, which is expected to accurately characterize the semantic relationship of samples. In Fig. 8, some EEG sample pairs are respectively utilized to show the similarity learning of GASDSL. That is, the gradually increasing and decreasing similarity values respectively corresponding to the within-class and between-class cases are found in these two subfigures.

3.4.3. Parameter sensitivity analysis

This section investigates the performance of GASDSL in terms of the model parameters. There are three parameters in GASDSL, *i.e.*, α, β, and m, in order to balance the impacts of respective terms. Specifically, α controls the impact of graph similarity matrix learning and β is associated with the entropy regularization, and m is the subspace dimensionality. Fig. 9 corresponds to the case of 'subject1: session1→session2' from SEED-IV, where we show the performance variations of GASDSL in terms of two among the three parameters by fixing the third one m, β, α respectively as 30, $2^8, 2^9$. Obviously, we find that GASDSL is slightly more sensitive to β than α and m. According to the definition of entropy regularization, different βs controls the number of neighboring samples for a certain EEG sample to connect, *i.e.*, the neighborhood size. Equivalently, it mainly functions for local data submanifold exploration. Due to the irregularity of EEG features and even the inter-session variabilities, the flexibility of parameter β coincides with our intuitive understanding to the EEG data properties. Generally, we can select α, β, m respectively from candidate values $\{2^7, 2^8, \cdots, 2^{12}\}, \{2^7, 2^8, \cdots, 2^{11}\}$ and $\{20, 30, \cdots, 100\}$ to make GASDSL achieve good performance.

3.5. Insights into the EEG spatial-frequency patterns

In the above two sections, we have confirmed that GASDSL not only improves the emotion recognition accuracy, but also identifies the discriminative subspace, from pattern classification perspective. Below we take a closer look at the contributions of different EEG features and further the different frequency bands and channels in emotion recognition. To this end, we should first

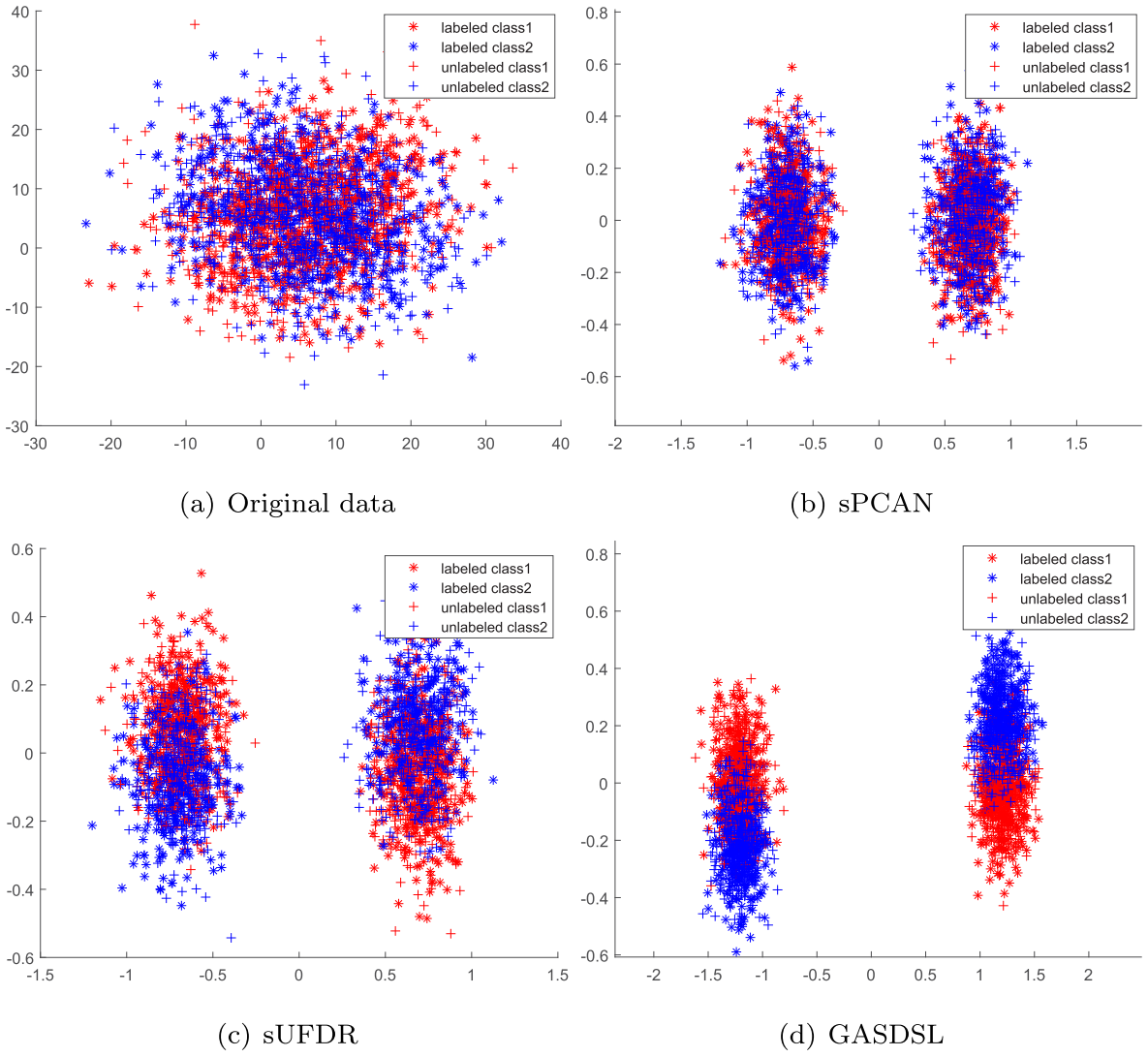

Fig. 6. Subspace learning on a synthetic dataset with large noises.

quantitatively calculate the importance of all feature dimensions on one hand; on the other hand, we should build the correspondence between EEG frequency bands (channels) and feature dimensions.

We propose to use the normalized ℓ_2-norm of each row of the learned projection matrix in GASDSL to serve as the quantitative importance of each feature dimension. Specifically, we calculate the importance of the i-th EEG feature, $\theta_i|_{i=1}^{d}$, by

$$\theta_i = \frac{\|\mathbf{w}^i\|_2}{\sum_{j=1}^{d}\|\mathbf{w}^j\|_2}, \tag{23}$$

where $\mathbf{w}^i$ is the i-th row of the projection matrix $\mathbf{W}$. Obviously, the larger θ_i, the more discriminative the i-th EEG feature dimension in differentiating emotional states. If we have p EEG frequency bands and q channels, according to the established correspondence between EEG frequency bands (channels) and feature dimensions (Peng et al., 2022b), the importance of the $i|_{i=1}^{p}$-th frequency band can be calculate by

$$\omega(i) = \theta_{(i-1)\times q+1} + \theta_{(i-1)\times q+2} + \ldots + \theta_{i\times q}. \tag{24}$$

Similarly, the importance of the $j|_{j=1}^{q}$-th channel can be calculated by

$$\psi(i) = \theta_j + \theta_{j+q} + \ldots + \theta_{j+(p-1)\times q}. \tag{25}$$

There are 62 EEG channels and five frequency bands in both SEED-IV and SEED-V. Therefore, we respectively set p to 5 and q to 62 in the rules (24) and (25). The average results of EEG frequency bands across the three cross-session emotion recognition settings on these two datasets are presented as bar plots in Figs. 10a) and 11a). According to our results, features extracted from the *Gamma* band play the most important roles in emotion recognition. Such data-driven results might be explained from two aspects. One is that the *Gamma* band indeed correlates more to the neural mechanism of affective information processing and the other is that the *Gamma* band contains the broadest frequency interval (*i.e.*, 31–50 Hz) among the five bands.

Based on the rule (25), we obtain the importance values of different EEG channels. By visualizing the EEG channel importance values by the form of brain topology in Figs. 10b), we gain some insights into the discriminative abilities of different brain regions in emotion recognition. We conclude that the left/right temporal, prefrontal, and (central) parietal lobes are identified to be more correlated to emotion expression. The above critical frequency bands and channels identification results are generally consistent with some existing studies (Peng et al., 2022b; Zheng and Lu, 2015; Zheng et al., 2019).

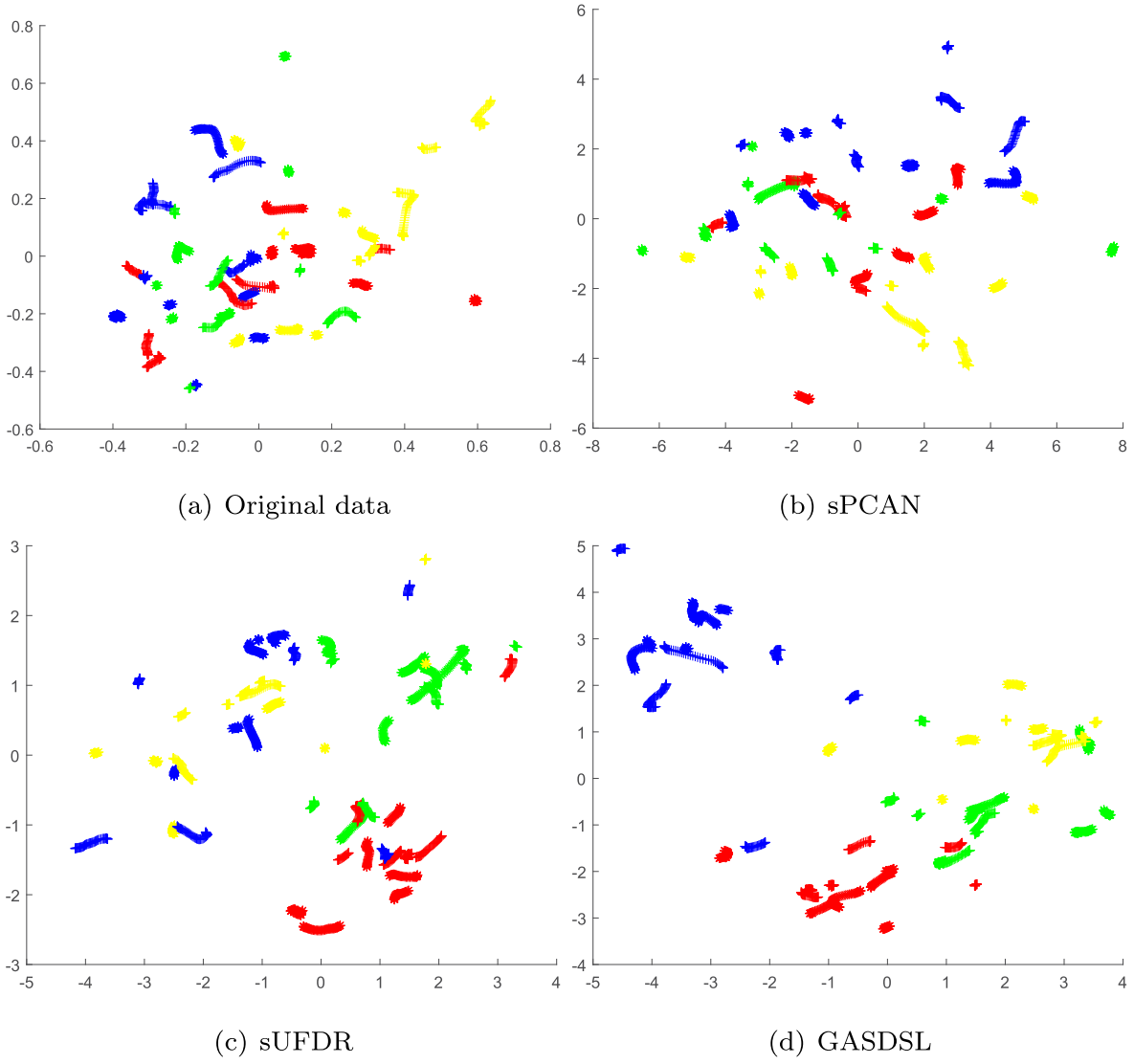

(a) Original data (b) sPCAN

(c) sUFDR (d) GASDSL

Fig. 7. Subspace learning of different models on an example EEG emotion recognition case 'subject 15: session1→session2'.

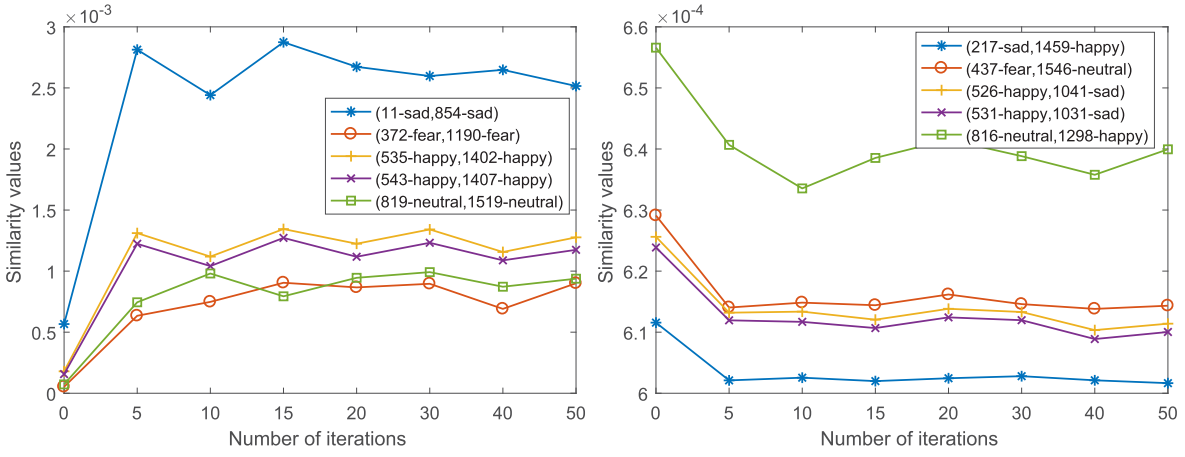

(a) Within-class samples (b) Between-class samples

Fig. 8. Similarity learning of sample pairs in the maximum entropy graph.

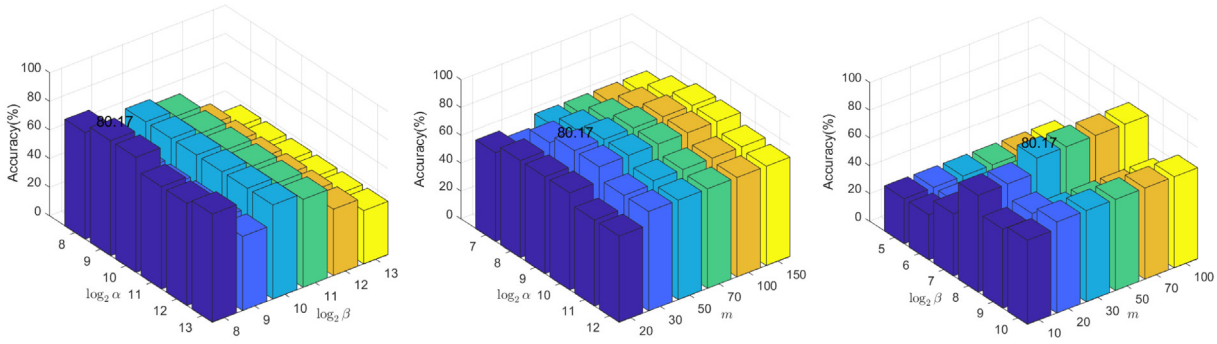

(a) Accuracy vs. (α, β) (b) Accuracy vs. (α, m) (c) Accuracy vs. (β, m)

Fig. 9. Parameter sensitivity analysis on an example case of 'subject 1: session 1→session 2' in SEED-IV.

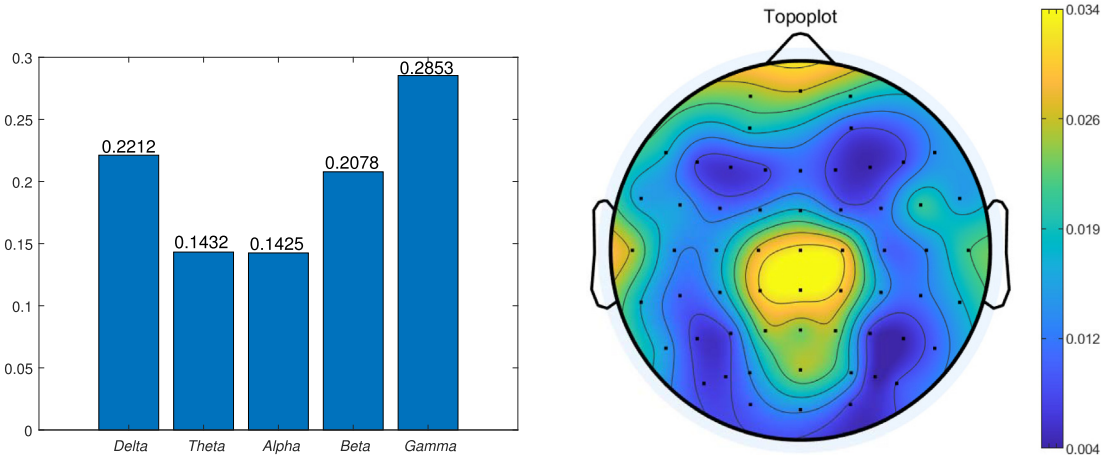

(a) frequency bands (b) channels

Fig. 10. Analysis of affective activation patterns in SEED-IV.

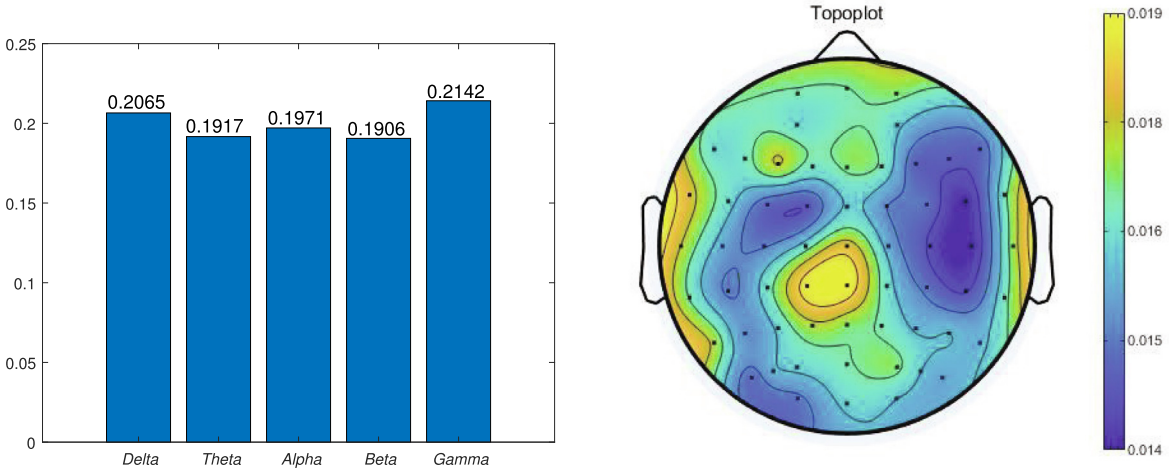

(a) frequency bands (b) channels

Fig. 11. Analysis of affective activation patterns in SEED-V.

4. Discussions

What these models have in common are three folds. First, they are all joint models to unify some sub-tasks together by different strategies. For example, PCAN can be seen as a joint model for structured graph learning and spectral clustering. Second, all of them are closely related to graph construction. In sPCAN, graph learning is enforced to satisfy three properties of non-negativity, row-normalization and rank constraint while in both sMEG and GASDSL, the rank constraint is replaced by the entropy regularizer. Though there is not explicit graph learning in sUFDR, the dimensionality reduction step is equivalent to the strategy that first constructs a graph via the given and estimated data labels and then finds a subspace to preserve the data structure information depicted by this graph, according to the spectral regression theory (Peng et al., 2020). Third, all these models involve subspace learning for graph construction or label prediction.

The differences between GASDSL and each of the other models are described below.

- In sPCAN, the structured graph learning process is unsupervised, which cannot make full use of the given label information of data. Though the pseudo-cluster assignment of data is coupled with the graph learning, the cluster indicator matrix is in real-valued coding, which is not capable enough in guiding the graph learning from our point of view.
- In both sPCAN and sMEG, the graph construction serves as the central place. That is, subspace learning aims to more accurately characterize the similarity between samples and then it is expected to obtain more accurate label propagation performance. However, in GASDSL, discriminative subspace learning acts the central role, whose learning process is mediated by both the graph learning and the semi-supervised label prediction processes.
- sUFDR uses an iterative way to explore the discriminative subspace and predict the label of unlabeled samples. Though it is termed an unified framework for dimensionality reduction, it has no unified objective function. The dimensionality reduction in sUFDR is only guided by the given and estimated data label information.
- In both sPCAN and sMEG, the label propagation on learned graph is usually restricted within the transductive paradigm and has no out-of-sample extension ability. That is, it is often necessary to contruct a new graph again when given a new sample. However, based on the learned subspace projection matrix and centroid, our proposed GASDSL can preform label prediction on unseen samples.

5. Conclusion and future work

In this paper, we proposed a Graph Adaptive Semi-supervised Discriminative Subspace Learning (GASDSL) model for recognizing emotional states from EEG data. GASDSL projected EEG data into a discriminative subspace to decrease the intra-class scatter and simultaneously increase inter-class separability. Moreover, we employed an adaptive graph construction component and a semi-supervised emotional state prediction component to mediate the discriminative subspace learning. The adaptive graph not only adopted the maximum entropy regularizer to exploit local structural information of EEG data, but also combined discriminative subspace learning into a single objective function to avoid the sub-optimality problem. In the learned discriminative subspace, the emotional state prediction of a certain sample was effectively achieved by discovering its nearest emotional state center. Based on the experimental results on the SEED-IV and SEED-V datasets, we concluded that 1) the joint learning strategy in GASDSL effectively improved the emotion recognition performance; 2) both the learned subspace and the maximum graph are discriminative for depicting the semantic information of EEG samples; and 3) the spatial-frequency patterns (*i.e.*, key EEG frequency bands and brain regions) in emotion recognition are quantitatively analyzed by the learned projection matrix. In the future, we will continue investigating the graph-based learning models for issues within EEG-based emotion recognition. Specifically, we will attempt to deal with the inter-subject variabilities in cross-subject EEG emotion recognition, *i.e.*, the bipartite graph-based adaptive data transferability quantification in cross-subject EEG emotion recognition (Li et al., 2022g). We will continue to explore discriminantive subspace learning guided by adaptive graphs, and attempt to solve the problem of emotion recognition in the case of multimodal data.

Declaration of Competing Interest

The authors declare that they have no known competing financial interests or personal relationships that could have appeared to influence the work reported in this paper.

Acknowledgement

This work was partially supported in part by the National Natural Science Foundation of China under Grant 61971173, Grant 61972121 and Grant U20B2074, and in part by the Natural Science Foundation of Zhejiang Province under Grant LY21F030005, and in part by the Key Research and Development Project of Zhejiang Province under Grant 2023C03026, Grant 2021C03001, and Grant 2021C03003.

References

Chen, X., Yuan, G., Nie, F., Huang, J.Z., 2017. Semi-supervised feature selection via rescaled linear regression. In: Proc. Int. J. Conf. Artif. Intell., pp. 1525–1531.
Chen, X., Yuan, G., Nie, F., Ming, Z., 2020. Semi-supervised feature selection via sparse rescaled linear square regression. IEEE Trans. Knowl. Data Eng. 32, 165–176.
Dadebayev, D., Goh, W., Tan, E., 2022. EEG-based emotion recognition: Review of commercial EEG devices and machine learning techniques. J. King Saud Univ. Comput. Inf. Sci. 34, 4385–4401.
Gao, Y., Sun, X., Meng, M., Zhang, Y., 2022. EEG emotion recognition based on enhanced SPD matrix and manifold dimensionality reduction. Comput. Biol. Med. 146, 105606.
Gong, S., Xing, K., Cichocki, A., Li, J., 2022. Deep learning in EEG: Advance of the last ten-year critical period. IEEE Trans. Cogn. Develop. Syst. 14, 348–365.
Gu, X., Cao, Z., Jolfaei, A., Xu, P., Wu, D., Jung, T., Lin, C., 2021. EEG-based brain-computer interfaces (BCIs): A survey of recent studies on signal sensing technologies and computational intelligence approaches and their applications. IEEE/ACM Trans. Comput. Biol. Bioinform. 18, 1645–1666.
Islam, M.R., Ahmad, M., 2019. Wavelet analysis based classification of emotion from EEG signal. In: Int. Conf. Electr., Comput. Commun. Eng., pp. 1–6.
Jiang, Y., Wu, D., Deng, Z., Qian, P., Wang, J., Wang, G., Chung, F., Choi, K., Wang, S., 2017. Seizure classification from EEG signals using transfer learning, semi-supervised learning and TSK fuzzy system. IEEE Trans. Neural Syst. Rehabil. Eng. 25, 2270–2284.
Jin, J., Sun, H., Daly, I., Li, S., Liu, C., Wang, X., Cichocki, A., 2022. A novel classification framework using the graph representations of Electroencephalogram for motor imagery based brain-computer interface. IEEE Trans. Neural Syst. Rehabil. Eng. 30, 20–29.
Kakkos, I., Dimitrakopoulos, G., Sun, Y., Yuan, J., Matsopoulos, G., Bezerianos, A., Sun, Y., 2021. EEG fingerprints of task-independent mental workload discrimination. IEEE J. Biomed. Health Informat. 25, 3824–3833.
Kalantar, G., Mohammadi, A., 2018. Graph-based dimensionality reduction of EEG signals via functional clustering and total variation measure for BCI systems. In: Proc. Annu. Int. Conf. IEEE Eng. Med. Biol. Soc., pp. 4603–4606.
Leng, L., Zhang, J., 2013. Palmhash code vs. palmphasor code. Neurocomputing 108, 1–12.
Leng, L., Zhang, J., Khan, M.K., Chen, X., Alghathbar, K., 2010. Dynamic weighted discrimination power analysis: A novel approach for face and palmprint recognition in DCT domain. Int. J. Phys. Sci. 5, 2543–2554.
Leng, L., Zhang, J., Chen, G., Khan, M.K., Alghathbar, K., 2011. Two-directional two-dimensional random projection and its variations for face and palmprint recognition. Commun. Sys. Appl., pp. 458–470.
Leng, L., Zhang, S., Bi, X., Khan, M.K., 2012. Two-dimensional cancelable biometric scheme. In: Int. Conf. Wavelet Anal. Pattern Recognit., pp. 164–169.
Leng, L., Li, M., Kim, C., Bi, X., 2017. Dual-source discrimination power analysis for multi-instance contactless palmprint recognition. Multimedia Tools Appl. 76, 333–354.

Li, X., Zhang, H., Zhang, R., Liu, Y., Nie, F., 2018. Generalized uncorrelated regression with adaptive graph for unsupervised feature selection. IEEE Trans. Neural Netw. Learn. Syst. 30, 1587–1595.
Li, J., Thakor, N., Bezerianos, A., 2020. Brain functional connectivity in unconstrained walking with and without an exoskeleton. IEEE Trans. Neural Syst. Rehabil. Eng. 28, 730–739.
Li, C., Wang, B., Zhang, S., Liu, Y., Song, R., Cheng, J., Chen, X., 2022a. Emotion recognition from EEG based on multi-task learning with capsule network and attention mechanism. Comput. Biol. Med. 143, 105303.
Li, G., Chen, N., Jin, J., 2022b. Semi-supervised EEG emotion recognition model based on enhanced graph fusion and GCN. J. Neural Eng. 19, 026039.
Li, J., Hua, H., Xu, Z., Shu, L., Xu, X., Kuang, F., Wu, S., 2022c. Cross-subject EEG emotion recognition combined with connectivity features and meta-transfer learning. Comput. Biol. Med. 145, 105519.
Li, R., Ren, C., Zhang, X., Hu, B., 2022d. A novel ensemble learning method using multiple objective particle swarm optimization for subject-independent EEG-based emotion recognition. Comput. Biol. Med. 140, 105080.
Li, X., Zhang, Y., Tiwari, P., Song, D., Hu, B., Yang, M., Zhao, Z., Kumar, N., 2022e. EEG based emotion recognition: A tutorial and review. ACM Comput. Surv. 55 (79), 1–57.
Li, Y., Zheng, W., Wang, L., Zong, Y., Cui, Z., 2022f. From regional to global brain: A novel hierarchical spatial-temporal neural network model for EEG emotion recognition. IEEE Trans. Affect. Comput. 13, 568–578.
Li, Z., Zhu, E., Jin, M., Fan, C., He, H., Cai, T., Li, J., 2022g. Dynamic domain adaptation for class-aware cross-subject and cross-session EEG emotion recognition. IEEE J. Biomed. Health Informat. 26, 5964–5973.
Liu, W., Qiu, J., Zheng, W., Lu, B., 2022. Comparing recognition performance and robustness of multimodal deep learning models for multimodal emotion recognition. IEEE Trans. Cogn. Develop. Syst. 14, 715–729.
Nie, F., Wang, X., Huang, H., 2014. Clustering and projected clustering with adaptive neighbors. In: Proc. ACM SIGKDD Int. Conf. Knowl. Disc. Data Min., pp. 977–986.
Nie, F., Zhao, X., Wang, R., Li, X., 2023. Adaptive maximum entropy graph-guided fast locality discriminant analysis. IEEE Trans. Cybern. 53, 3574–3687.
Peng, Y., Zhang, L., Kong, W., Qin, F., Zhang, J., 2020. Joint low-rank representation and spectral regression for robust subspace learning. Knowl.-Based Syst. 195, 105723.
Peng, Y., Jin, F., Kong, W., Nie, F., Lu, B., Cichocki, A., 2022a. OGSSL: A semi-supervised classification model coupled with optimal graph learning for EEG emotion recognition. IEEE Trans. Neural Sys. Rehabil. Eng. 30, 1288–1297.
Peng, Y., Qin, F., Kong, W., Ge, Y., Nie, F., Cichocki, A., 2022b. GFIL: a unified framework for the importance analysis of features, frequency bands and channels in EEG-based emotion recognition. IEEE Trans. Cognit. Develop. Syst. 14, 935–947.
Peng, Y., Zhang, Y., Kong, W., Nie, F., Lu, B., Cichocki, A., 2022c. S^3LRR: A unified model for joint discriminative subspace identification and semisupervised eeg emotion recognition. IEEE Trans. Instrum. Meas. 71, 1–13.
Shang, R., Zhang, X., Feng, J., Li, Y., Jiao, L., 2022. Sparse and low-dimensional representation with maximum entropy adaptive graph for feature selection. Neurocomputing 485, 57–73.
Tang, J., Liu, D., Jin, X., Peng, Y., Zhao, Q., Ding, Y., Kong, W., 2023. BAFN: Bi-direction attention based fusion network for multimodal sentiment analysis. IEEE Trans. Circuits Syst. Video Technol. 33, 1966–1978.
Wang, H., Liu, X., Hu, H., Wan, F., Li, T., Gao, L., Bezerianos, A., Sun, Y., Jung, T.-P., 2020. Dynamic reorganization of functional connectivity unmasks fatigue related performance declines in simulated driving. IEEE Trans. Neural Syst. Rehabil. Eng. 28, 1790–1799.
Wang, C., Chen, X., Yuan, G., Nie, F., Yang, M., 2022a. Semisupervised feature selection with sparse discriminative least squares regression. IEEE Trans. Cybern. 52, 8413–8424.
Wang, J., Ma, Z., Nie, F., Li, X., 2022b. Entropy regularization for unsupervised clustering with adaptive neighbors. Pattern Recogn. 125, 108517.
Wang, Q., Wang, M., Yang, Y., Zhang, X., 2022c. Multi-modal emotion recognition using EEG and speech signals. Comput. Biol. Med. 149, 105907.
Wei, Y., Liu, Y., Li, C., Cheng, J., Song, R., Chen, X., 2023. TC-Net: A transformer capsule network for EEG-based emotion recognition. Comput. Biol. Med. 152, 106463.
Wu, T., Xiao, Y., Guo, M., Nie, F., 2020. A general framework for dimensionality reduction of k-means clustering. J. Classif. 37, 616–631.
Wu, Y., Xia, M., Nie, L., Zhang, Y., Fan, A., 2022. Simultaneously exploring multi-scale and asymmetric eeg features for emotion recognition. Comput. Biol. Med. 149, 106002.
Wu, M., Teng, W., Fan, C., Pei, S., Li, P., Lv, Z., 2023. An investigation of olfactory-enhanced video on EEG-based emotion recognition. IEEE Trans. Neural Syst. Rehabil. Eng., 1602–1613
Zhang, G., Yu, M., Chen, G., Han, Y., Zhang, D., Zhao, G., Liu, Y., 2019. A review of EEG features for emotion recognition. Scientia Sinica Informat. 49, 1097–1118.
Zhang, J., Wei, Z., Zou, J., Fu, H., 2020a. Automatic epileptic EEG classification based on differential entropy and attention model. Eng. Appl. Artif. Intell. 96, 1–10.
Zhang, R., Li, X., Zhang, H., Nie, F., 2020b. Deep fuzzy k-means with adaptive loss and entropy regularization. IEEE Trans. Fuzzy Syst. 28, 2814–2824.
Zheng, W., Lu, B., 2015. Investigating critical frequency bands and channels for EEG-based emotion recognition with deep neural networks. IEEE Trans. Auton. Mental Develop. 7, 162–175.
Zheng, J., Yang, P., Chen, S., Shen, G., Wang, W., 2017. Iterative re-constrained group sparse face recognition with adaptive weights learning. IEEE Trans. Image Process. 26, 2408–2423.
Zheng, W., Liu, W., Lu, Y., Lu, B., Cichocki, A., 2018. Emotionmeter: A multimodal framework for recognizing human emotions. IEEE Trans. Cybern. 49, 1110–1122.
Zheng, W., Zhu, J., Lu, B., 2019. Identifying stable patterns over time for emotion recognition from EEG. IEEE Trans. Affect. Comput. 10, 417–429.
Zhong, W., Chen, X., Nie, F., Huang, J.Z., 2021. Adaptive discriminant analysis for semi-supervised feature selection. Inf. Sci. 566, 178–194.